Defect-controlled electronic transport in single, bilayer, and N-doped graphene: Theory

K. Carva,[1,2] B. Sanyal,[1] J. Fransson,[1] and O. Eriksson[1]
[1]*Uppsala University, Department of Physics and Astronomy, Division of Materials Theory, P.O. Box 516, SE-75120 Uppsala, Sweden*
[2]*Charles University, Faculty of Mathematics and Physics, Department of Condensed Matter Physics, CZ-12116 Prague 2, Czech Republic*
(Received 9 December 2009; published 2 June 2010)

We report on a theoretical study of the electronic-structure and transport properties of single and bilayer graphene with vacancy defects, as well as N-doped graphene. The theory is based on first-principles calculations as well as model investigations in terms of real-space Green's functions. We show that increasing the defect concentration increases drastically the conductivity in the limit of zero applied gate voltage, by establishing carriers in originally carrier-free graphene, a fact which is in agreement with recent observations. We calculate the amount of defects needed for a transition from a nonconducting to a conducting regime (i.e., a metal-insulator transition) and establish the threshold of the defect concentration where the increase in impurity scattering dominates over the increase in carrier-induced conductivity.

DOI: 10.1103/PhysRevB.81.245405 PACS number(s): 72.80.Vp, 73.22.Pr, 71.30.+h

I. INTRODUCTION

Graphene as a zero-gap semiconductor/semimetal represents physically a very interesting system. The physical and chemical properties of graphene have raised a lot of attention with reports of unique structural and electronic properties.[1–3] Since the discovery of graphene, one may have witnessed an increased focus on chemical functionalization and the possibility to influence the electronic properties by means of adatoms, impurities, or geometrical confinement. It has, for instance, been shown that the electronic structure of graphene can be influenced by the insertion of defects using a chemical treatment.[4] The possibility to open band gaps, induce gap states by defects, and the ability to control the conductivity, in general, by chemical and physical means must be viewed as a crucial step, in order to establish graphene as a competitive material for electronics applications. We are as a matter of fact already witnessing several applications of graphene, for instance, the ability as a material for use in gas detectors, where the capability to detect the adsorption of single gas atoms has been demonstrated.[5]

Initial steps in the direction of modifying the electronics properties of graphene by means of chemical functionalization have been reported. For instance, the electronic structure of acid-treated Graphene was studied by means of x-ray absorption spectroscopy and first-principles theory,[4] and it was argued that defects introduced in the acid treatment modified the electronic structure drastically. In a paper subsequent to the work of Coleman *et al.*[4] it was shown experimentally and theoretically that the conductivity of graphene can also be drastically modified by the introduction of the defects.[6] The reason for this was argued to be partly due to so-called midgap states[7] being introduced due to the defects and these midgap states provide a metallic character of the electronic structure in a region located around the defect site. Both single and double vacancies were considered in the theoretical work, as well as vacancies dressed by atomic species which saturate dangling bonds. It was found that for all calculations a metallic component to the density of states (DOS) develops with the creation of the defects. Furthermore, a theoretical study of Sanyal *et al.*[8] show that it may be possible to incorporate molecular nitrogen into defected graphene, especially at divacancy sites. At such defects nitrogen was argued to enter and take positions of the C honeycomb lattice hence repairing the defected C lattice perfectly. Since this involves a replacement of C atoms with N atoms, with one extra valence electron, it was argued that this is an efficient way to dope graphene with electron states.

In this paper we focus on the theory of the electronic-structure and the transport properties of graphene, both as a single layer as well as a bilayer, as a function of defect concentration. Both tight-binding model results and first-principles calculations are presented and support the main conclusions of the paper. We also consider the transport properties of graphene as a function of N defects, along the ideas suggested in Ref. 8.

II. THEORY

The primary theoretical tool employed here was an all-electron scalar-relativistic version of the tight-binding linear muffin-tin orbital (LMTO) method[9] within the local spin-density approximation.[10] The valence basis consisted of *s*, *p*, and *d* orbitals. The atomic sphere approximation was employed, which required an additional empty sphere to be present in the graphene layer per two carbon atoms and other empty spheres between graphene layers with a spatial distribution similar to the one already used successfully for graphite.[11] The integrations over the two-dimensional Brillouin zone were performed on a uniform mesh of about 5000 $\mathbf{k}_{\parallel}$ points. Such high density of $\mathbf{k}_{\parallel}$ mesh is crucial for the accurate description of states near the Dirac point.

The random distribution of defects in the system is described by means of the coherent potential approximation (CPA).[12,13] This single-site approximation has been shown to be successful in predicting both ground-state and transport properties[14] of systems with random disorder, thus averaged over all possible combinations of impurity distributions. The CPA can deal with systems with arbitrary low concentration of impurities while its numerical requirements remain mod-

est compared to the supercell method for disordered systems. The CPA has been used in other studies of graphene, where it was argued that it gives very good results for the physical properties of graphene.[15,16] The applicability of the CPA near the Dirac point was analyzed by Skrypnyk and Loktev.[17] They noted that only renormalized approaches, such as the CPA, can be efficient close to the van Hove singularities in the spectrum. Furthermore, it was found that in the vicinity of the Dirac point a correction to the CPA self-energy is needed. We study here the DOS and conductivity only for systems with a finite concentration of impurities, which naturally induces a shift of the Fermi level away from the Dirac point, which improves the conditions for CPA applicability. The conductance was calculated from the Kubo linear-response theory. Our calculation cannot provide an accurate description of the critical behavior at the predicted metal-insulator transition since that cannot be expected from a mean-field theory but quantitative predictions for a region of concentration further away from this transition should be accurate and still interesting, for example, to compare the effect of different impurities.

We also investigated the electronic structure of graphene by means of *ab initio* self-consistent density-functional theory[18] calculations, using the Vienna *ab initio* simulation package (VASP).[19,20] These calculations employed the projector augmented wave method and the plane wave cut-off energy was set to 750 eV. The generalized gradient approximation was used for the treatment of exchange-correlation functional. A lateral $8\times8\times1$ supercell of graphene with a divacancy was considered for the calculation of single layer and a $5\times5\times2$ supercell for the bilayer calculation. The geometry of the supercell in presence of the defect was optimized by minimizing Hellmann-Feynman forces with a tolerance of 0.01 eV/Å. A Γ-centered $3\times3\times1$ set of k points was used in the Monkhorst-Pack scheme with a Gaussian broadening of 0.2 eV. *Ab initio* calculations are complemented by detailed model calculations of the electronic properties of graphene, using tight-binding theory expressed in second quantized form, a Green's function (GF) formalism as well as the Kubo formula for transport properties.

III. RESULTS

A. Model of the bilayer graphene with a single defect

The model calculations considered the electronic-structure and transport properties of defects in a bilayer of graphene. We model the electronic structure of this graphene bilayer with a nearest-neighbor Hamiltonian system

$$\mathcal{H}_0 = -t\sum_{\langle ij\rangle\sigma}[a_{i\sigma}^\dagger b_{j\sigma} + c_{i\sigma}^\dagger d_{j\sigma}] - t_\perp \sum_{\langle ij\rangle\sigma} b_{i\sigma}^\dagger d_{j\sigma} + \text{H.c.} \quad (1)$$

Here and henceforth, we will refer to the upper (lower) layer as the one in which the operators $a_{i\sigma}, b_{i\sigma}$ ($c_{i\sigma}, d_{i\sigma}$) act. Moreover, the upper (lower) layer can be thought of as two sublattices in which the respective operators $a_{i\sigma}$ and $b_{i\sigma}$ ($c_{i\sigma}$ and $d_{i\sigma}$) act. The sublattices are coupled by the first term in Eq. (1) whereas the two layers are coupled through the second term.

By introducing the band operators $a_{\mathbf{k}\sigma}^\dagger$ via the transformation $a_{i\sigma}^\dagger = \Sigma_{\mathbf{k}} a_{\mathbf{k}\sigma}^\dagger e^{i\mathbf{k}\cdot\mathbf{r}_i}/\sqrt{N}$, etc., we rewrite the model according to

$$\mathcal{H}_0 = \sum_{\mathbf{k}\sigma} \phi(\mathbf{k})[a_{\mathbf{k}\sigma}^\dagger b_{\mathbf{k}\sigma} + c_{\mathbf{k}\sigma}^\dagger d_{\mathbf{k}\sigma}] - t_\perp \sum_{\mathbf{k}\sigma} b_{\mathbf{k}\sigma}^\dagger d_{\mathbf{k}\sigma} + \text{H.c.}, \quad (2)$$

where $\phi(\mathbf{k}) = -t\Sigma_{i=1}^3 e^{i\mathbf{k}\cdot\boldsymbol{\delta}_i}$. Here, e.g.,

$$\boldsymbol{\delta}_1 = \frac{a}{2}(1,\sqrt{3},0), \quad \boldsymbol{\delta}_2 = a(-1,0,0), \quad \boldsymbol{\delta}_3 = \frac{a}{2}(1,-\sqrt{3},0) \quad (3)$$

with the in-plane lattice parameter a and out-of-plane lattice parameter c. Typically $t_\perp \sim t/10$. We further introduce a single impurity at the position $\mathbf{r}_0$ in the upper layer through $\mathcal{H}_{\text{imp}} = V_0 \Sigma_\sigma a_{0\sigma}^\dagger a_{0\sigma}$, and we study how this impurity influences the electronic structure and transport properties of the upper and lower layer. The Dirac points are given at $K = 2\pi(1, 1/\sqrt{3})/3a$ and $K' = 2\pi(1, -1/\sqrt{3})/3a$. We linearize the dispersion around the Dirac point, for which we have, e.g., $\phi(\mathbf{k}+\mathbf{K}) \simeq v_F(k_y - ik_x)e^{i\pi/3} = v_F k e^{i(\pi/3+\varphi)}$, where $v_F = 3at/2$, $k = |\mathbf{k}|$, and $\tan\varphi = -k_x/k_y$.

Ultimately, we seek to calculate the spatial dependence of the local DOS (LDOS) and the conductivity in both layers, for which we employ the real-space GF $\mathbf{G}(\mathbf{r},\mathbf{r}';i\omega)$. The spatially resolved local DOS, $\rho(\mathbf{r};\omega)$, is obtained from the GF by calculating $\rho(\mathbf{r};\omega) = -\text{Tr Im}\,\mathbf{G}^r(\mathbf{r},\mathbf{r};\omega)/\pi$, where the superscript r denotes the retarded GF, whereas the main qualitative features of the conductivity can be calculated using the Kubo formula.

We expand the real-space GF in terms of the homogeneous GF $\mathbf{G}_0(\mathbf{r}-\mathbf{r}';i\omega) = \int \mathbf{G}_0(\mathbf{k};i\omega)e^{-i\mathbf{k}\cdot(\mathbf{r}-\mathbf{r}')}d\mathbf{k}/(2\pi)^2$ and the T-matrix equation

$$\mathbf{G}(\mathbf{r},\mathbf{r}') = \mathbf{G}_0(\mathbf{r}-\mathbf{r}') + \mathbf{G}_0(\mathbf{r}-\mathbf{r}_0)\mathcal{T}(\mathbf{r}_0)\mathbf{G}_0(\mathbf{r}_0-\mathbf{r}'). \quad (4)$$

The bare GF $\mathbf{G}_0(\mathbf{k};i\omega)$ satisfies the equation of motion

$$\begin{pmatrix} i\omega & -\phi & 0 & 0 \\ -\phi^* & i\omega & 0 & t_\perp \\ 0 & 0 & i\omega & -\phi \\ 0 & t_\perp & -\phi^* & i\omega \end{pmatrix} \mathbf{G}_0(\mathbf{k};i\omega) = 1 \quad (5)$$

and can be written

$$\mathbf{G}_0(\mathbf{k};i\omega) = \frac{q^{-1}}{q^{-2} - (i\omega)^2 t_\perp^2} \begin{pmatrix} \mathbf{A}(\mathbf{k};i\omega) & \mathbf{C}(\mathbf{k};i\omega) \\ \mathbf{C}(\mathbf{k};i\omega) & \mathbf{A}(\mathbf{k};i\omega) \end{pmatrix}, \quad (6)$$

where

$$\mathbf{A}(\mathbf{k};i\omega) = \begin{pmatrix} i\omega(1-t_\perp^2 q) & \phi \\ \phi^* & i\omega \end{pmatrix}, \quad (7)$$

$$\mathbf{C}(\mathbf{k};i\omega) = -qt_\perp \begin{pmatrix} |\phi|^2 & i\omega\phi \\ i\omega\phi^* & (i\omega)^2 \end{pmatrix} \quad (8)$$

$q = [(i\omega)^2 - |\phi|^2]^{-1}$. In terms of this GF and the impurity potential V_0, the T matrix can be analytically summed and reads

$$\mathcal{T} = [1 - \mathbf{V}_0\mathbf{G}_0]^{-1}\mathbf{V}_0 = T_0\ \mathrm{diag}\{1,0,0,0\},$$

$$T_0 = \frac{1}{V_0^{-1} - i\omega\int \frac{q^{-1} - t_\perp^2}{q^{-2} - (i\omega)^2 t_\perp^2}\frac{d\mathbf{k}}{(2\pi)^2}}, \tag{9}$$

where $\mathbf{V}_0 = V_0\ \mathrm{diag}\{1,0,0,0\}$. Here, $\mathrm{diag}\{d_1, d_2, \ldots, d_N\}$ denotes an N-dimensional diagonal matrix. In the low-energy regime, $|\omega| < t_\perp$, the integral in the denominator of T_0 is approximately given by

$$(i\omega)\int \frac{q^{-1} - t_\perp^2}{q^{-2} - (i\omega)^2 t_\perp^2}\frac{d\mathbf{k}}{(2\pi)^2} \to \{i\omega \to \omega + i\delta\} \to -F_0(\omega) - i\pi\rho_0(\omega), \tag{10}$$

where

$$F_0(\omega) = \frac{\omega}{8\pi v_F^2}\ln\frac{v_F^4 k_c^4}{\omega^2|\omega^2 - t_\perp^2|}, \tag{11a}$$

$$\rho_0(\omega) = \frac{|\omega|}{4\pi v_F^2}[1 + t_\perp/(2|\omega|)] \tag{11b}$$

whereas k_c is a momentum cutoff on the order of the inverse lattice spacing.[21]

The modification of the electronic structure in the upper (lower) layer due to the impurity is calculated by noting that only upper left (lower right) matrix in the product

$$\mathbf{G}_0\mathcal{T}\mathbf{G}_0 = \begin{pmatrix} \mathbf{ATA} & \mathbf{ATC} \\ \mathbf{CTA} & \mathbf{CTC} \end{pmatrix} \tag{12}$$

contributes, where $\mathbf{T} = T_0\ \mathrm{diag}\{1,0\}$. From this structure it is easy to see that we only need to calculate the GFs A_{11}, A_{12}, A_{21}, C_{11}, C_{12}, and C_{21}. For the low-energy regime, $|\omega| < t_\perp$, we find the approximate solutions

$$A_{11}(\mathbf{r},\mathbf{r}';\omega) = -J_0(k_F|\mathbf{r} - \mathbf{r}'|)[F_0(\omega) + i\pi\rho_0(\omega)], \tag{13a}$$

$$A_{12}(\mathbf{r},\mathbf{r}';\omega) = -J_1(k_F|\mathbf{r} - \mathbf{r}'|)v_F k_c e^{i5\pi/6}/(2\pi v_F^2), \tag{13b}$$

$$C_{11}(\mathbf{r},\mathbf{r}';\omega) = -t_\perp|\omega|^{-1}J_0(k_F|\mathbf{r} - \mathbf{r}'|)[F_0(\omega)\mathrm{sign}(\omega) - i\pi\rho_0(\omega)], \tag{13c}$$

$A_{21} = A_{12}e^{-i2\pi/3}$ and $C_{21}, C_{12} \approx 0$.

Around the Fermi level, $\omega = 0$, the only non-negligible propagators are $A_{11}(\omega) \sim -i\pi t_\perp J_0/(8\pi v_F^2)$, $A_{12}(\omega) \sim -k_c J_0/(2\pi v_F)$, and C_{11}. For the spatial correction to the density of electron states in the upper layer we note that $(x_0 = k_F|\mathbf{r} - \mathbf{r}_0|)$

$$-\frac{1}{\pi}\mathrm{Im}\ \mathbf{A}(\mathbf{r},\mathbf{r}_0)\mathbf{TA}(\mathbf{r}_0,\mathbf{r}) = -J_0(x_0)\begin{pmatrix} J_0(x_0)\rho_0 & \frac{v_F k_c}{(2\pi v_F)^2}J_1(x_0) \\ \frac{v_F k_c}{(2\pi v_F)^2}J_1(x_0) & 0 \end{pmatrix} + \frac{v_F k_c V_0^{-1}}{(V_0^{-1} + F_0)^2 + \pi^2\rho_0^2}\begin{pmatrix} J_0^2(x_0)\rho_0 V_0^{-1}/v_F k_c & J_0(x_0)J_1(x_0)\frac{V_0^{-1} + F_0 + \sqrt{3}\pi\rho_0}{(2\pi v_F)^2} \\ J_0(x_0)J_1(x_0)\frac{V_0^{-1} + F_0 - \sqrt{3}\pi\rho_0}{(2\pi v_F)^2} & \frac{k_c}{(2\pi v_F)^3}J_1^2(x_0)V_0\rho_0 \end{pmatrix} \tag{14}$$

whereas the analogous correction in the lower layer is given by

$$-\frac{1}{\pi}\mathrm{Im}\ \mathbf{C}(\mathbf{r},\mathbf{r}_0)\mathbf{TC}(\mathbf{r}_0,\mathbf{r}) = t_\perp^2 J_0^2(x_0)\frac{\rho_0}{\omega} \times \frac{[(V_0^{-1} + F_0)^2 - \pi^2\rho_0^2 - V_0^{-2}]/|\omega| + 2F_0^2\theta(\omega)/\omega}{(V_0^{-1} + F_0)^2 + \pi^2\rho_0^2}\begin{pmatrix} 1 & 0 \\ 0 & 0 \end{pmatrix}. \tag{15}$$

The effect of a defect created in a sublattice on the local DOS can now be qualitatively analyzed, and we notice in the upper layer the emergence of a midgap state in the other sublattice without the defect [b operators in Eq. (1)], which is expected from studies of single-layer graphene.[6,7,21] In agreement with previous theoretical studies on this level of approximation, the midgap state appears as a divergence in the local DOS as the defect potential $V_0 \to \infty$ for vanishing coupling $t_\perp$ between the layers, that is for a single-layer graphene. It is noticeable that a finite coupling strength removes the singularity. This behavior is expected since the electrons are not only interacting within the single-layer graphene but also with the adjacent second layer. Hence, lifetime effects due to this increased interaction with other electrons will arise from more than one source.

More important in the present context is that in the lower layer, which does not contain any defects, there is nevertheless a midgap state emerging, however, in the sublattice which does not couple to the upper layer [c operators in Eq. (1)]. In particular, letting the defect potential $V_0 \to \infty$, reduces the nonvanishing component in Eq. (15) to

$$t_\perp^2 J_0^2(x_0)\frac{\rho_0}{\omega}\frac{[F_0^2-\pi^2\rho_0^2]/|\omega|+2F_0^2\theta(\omega)/\omega}{F_0^2+\pi^2\rho_0^2}=\frac{t_\perp^2}{4\pi v_F^2}J_0^2(x_0)\frac{1}{\omega}\left[1+\frac{t_\perp}{2|\omega|}\right]\frac{[1+2\theta(\omega)]\ln^2\dfrac{v_F^2k_c^2}{|\omega|\sqrt{|\omega^2-t_\perp^2|}}-\pi^2\left[1+\dfrac{t_\perp}{2|\omega|}\right]^2}{\ln^2\dfrac{v_F^2k_c^2}{|\omega|\sqrt{|\omega^2-t_\perp^2|}}+\pi^2\left[1+\dfrac{t_\perp}{2|\omega|}\right]^2}, \quad (16)$$

which diverges like $1/\omega$ as $|\omega| \to 0$. Here, $\theta(\omega)$ is the step function. The divergence as such is an unphysical artifact of the approximations made in our model. Its presence does, nonetheless, indicate the emergence of the midgap state in the lower graphene layer which induces a metallicity around the defect with a length scale of the order of several lattice parameters.

Considering the electrical conductivity in the lower layer from the point of view of the Kubo formula, i.e.,

$$\sigma_{xx}^{ll}(\omega,\mathbf{k}) \sim \int [f(\varepsilon)-f(\varepsilon-\omega)][\mathrm{Im}\, G_c(\varepsilon)\mathrm{Im}\, G_d(\varepsilon-\omega) + \mathrm{Im}\, G_d(\varepsilon)\mathrm{Im}\, G_c(\varepsilon-\omega)]\frac{d\varepsilon}{2\pi}, \quad (17)$$

where the superscript ll denotes the lower layer whereas the subscript $c(d)$ signifies electrons of the different sublattices in the lower graphene layer. From this expression it becomes clear that the induced midgap state in the c sublattice, contributes to the conductivity in the lower layer, since the effect on the conductivity due to the defect provides the contribution

$$\delta\sigma_{xx}^{ll}(\omega,\mathbf{k}) \sim \int [f(\varepsilon)-f(\varepsilon-\omega)][\mathrm{Im}\, \delta G_c(\varepsilon)\mathrm{Im}\, G_d^{(0)}(\varepsilon-\omega) + \mathrm{Im}\, G_d^{(0)}(\varepsilon)\mathrm{Im}\, \delta G_c(\varepsilon-\omega)]\frac{d\varepsilon}{2\pi}. \quad (18)$$

Here, δG_c denotes the correction to the GF in the c sublattice comprising the defect-induced midgap state whereas $G_d^{(0)}$ is the bare GF for the d sublattice. For a dilute concentration of defects distributed in the upper layer, we thus expect that the conductivity should markedly rise as an effect of the emerging midgap state also in the lower layer, something that is verified with our numerical calculations, described below.

The theory can be improved employing, e.g., a full self-consistent Born approximation,[21] which is beyond the scope of the present paper. Instead we notice that the employed calculations provide a satisfactory qualitative description of the modified local DOS and the emergence of midgap states in both layers.

B. Results from first-principles theory

1. Electronic structure of graphene

To verify the predicted behavior from the theoretical models presented in the previous section, we will below present results from first-principles theory. As we shall see the model considerations and the numerical, materials specific calculations give a rather consistent picture of the influence of defects in the transport properties and electronic structure of graphene.

In Fig. 1 we show the DOS from our CPA calculations, for a single-atom-defect concentration of 0.1% and 1%, for a single graphene layer. In this figure we also display the DOS for defect-free graphene. It can be seen that the defects cause an increased number of states in the gap region between occupied and empty states. This is expected following the discussion about midgap states and the analysis presented in the section above. We will below be concerned mainly with the transport properties of single- and double-layer graphene, with and without defects, but we note already here that the DOS in Fig. 1 suggests an increased metallic component when the defect concentration increases, and hence a reduced resistivity.

The electronic structure shown in Fig. 1 was calculated using the CPA, and it is relevant to ask how reliable this theory is for describing the electronic structure and transport properties of graphene. In order to assess this we have calculated the DOS with and without defects. We subtracted the DOS curve of the impurity calculation from the DOS of ideal graphene. In this way we obtained the defect-induced features of the DOS, which give additional information compared to the DOS projected onto the vacancy empty sphere, shown in Fig. 1. We performed this calculation using the CPA as well as the supercell approach using a defect concentration of 1%. The result of the two calculations are shown in Fig. 2, the CPA LMTO calculation has been performed with a higher resolution than in the calculation for Fig. 1 in order to see finer details near the Dirac point. As may be seen from the figure, both the supercell calculation and the CPA calculation yield a midgap state, located in energy at the Dirac point. The intensity and width of the midgap state is quite similar from the two calculations, where the main difference is that the CPA method results, as is often the case, in a somewhat broadened midgap state, compared to the supercell results.

We have calculated the density of states of a bilayer graphene with a divacancy present only in one of the two

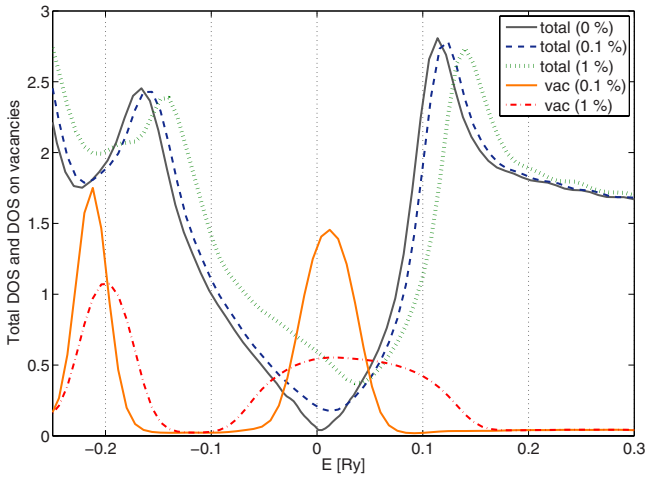

FIG. 1. (Color online) Calculated CPA-averaged DOS near the Fermi level: total and its contribution from vacancies for pure graphene and graphene with defect concentrations x=0.1% and 1%. Accuracy of this plot is lowered by artificial broadening because of the analytic continuation from complex energies, which is apparent at the Fermi level.

layers. These calculations have been performed employing VASP with the supercell approach as described in Sec. II. Geometry optimization gives rise to lattice distortions around the divacancy.[4,8] The results are presented in Fig. 3. One can observe prominent changes in the projected DOS for C atoms at different distances from a hole edge C atom present in the defected layer. The variation in local DOSs is also a consequence of sublattice effects.[6] The emergence of a midgap state also in the defect-free layer of the bilayer is in agreement with the tight-binding model calculation presented above. However, in this layer, the spatial variation in DOSs is very small. Sublattice and distance dependence of C sites from the hole edge C atom is very weak there. This is due to the weak interaction of this defect-free layer with the layer with defect which acts like an effective impurity. As there is a metallic component in both layers at the Fermi level, conductivity is increased as shown below.

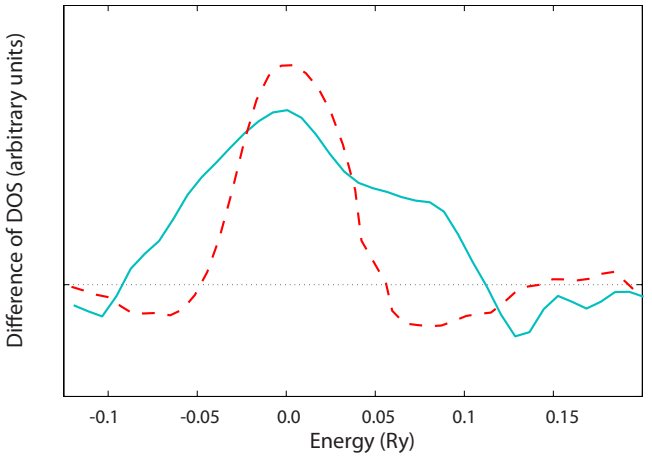

FIG. 2. (Color online) Calculated difference of graphene with and without defects (1%) using CPA (solid line, blue online) and the super cell approach (dashed line, red online).

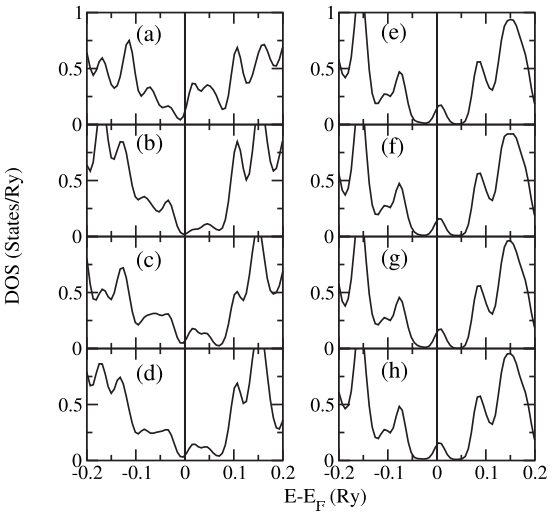

FIG. 3. Projected DOSs in the defected layer with the hole for C atoms situated at (a) 1.47 Å, (b) 3.91 Å, (c) 4.51, and (d) 6.39 Å from a C atom at the hole edge. The same for the layer without any defect for C atoms at distance (e) 4.14 Å, (f) 4.88, (g) 7.02 Å, and (h) 8.25 Å from the same hole edge C atom.

2. Transport properties of graphene

The calculated dependence of the resistivity, ρ, on vacancy concentration x is shown for graphene in Fig. 4. These results were obtained from a CPA, DFT in combination with the Kubo equation for the conductivity. It may be seen that the material exhibits a sharp drop in ρ for concentrations $x < 0.5\%$, which suggests an increasing metallic component in the DOS, which affects the resistivity of graphene. This result is in line with the DOS curves shown in Fig. 1. For values of x higher than 0.5%, the resistivity increases and its behavior is then similar to what is expected from a metallic material [where $\rho(x)$ slowly increases with defect concentration]. The results in Fig. 4 in fact show a transition from a semiconducting/semimetallic regime, with low conductivity, to a metallic regime, which takes place as a function of increasing defect concentration. Once the metallic regime has

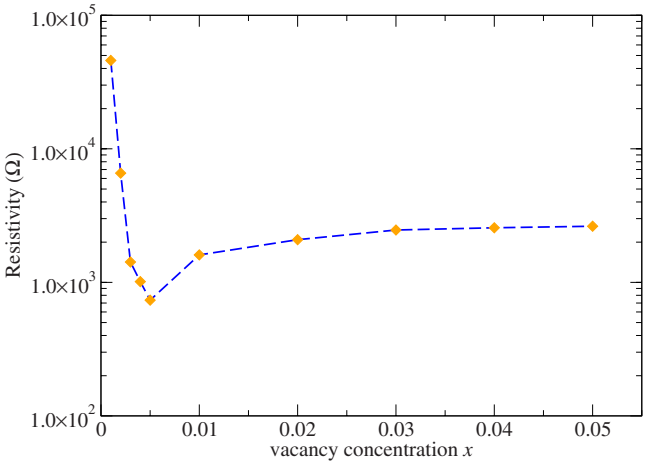

FIG. 4. (Color online) Calculated resistivity of a single layer of graphene as a function of vacancy concentration x.

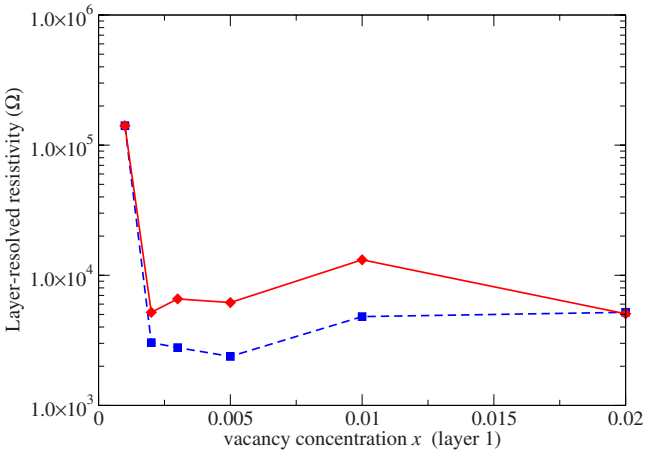

FIG. 5. (Color online) Calculated resistivity of individual layers of a graphene bilayer as a function of N impurity concentration x in the first layer while the amount of defects in the second layer is held fixed at 0.1%. Blue squares: resistivity of the first layer and red diamonds: resistivity of the second layer.

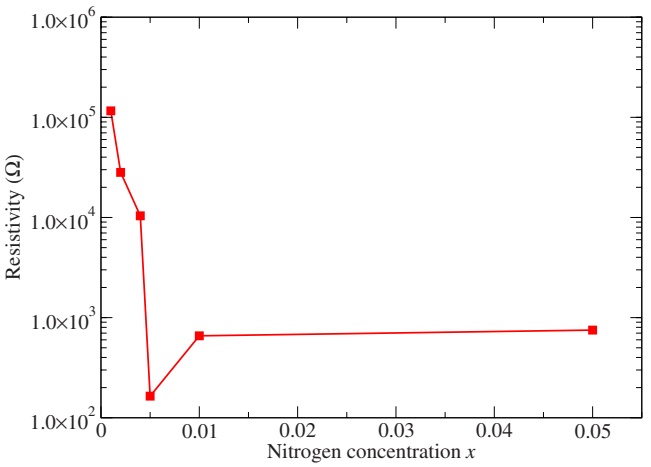

FIG. 6. (Color online) Calculated resistivity of a single layer of graphene as a function of N defect concentration x.

been established, a further increase in defects manifests themselves mainly as an increase in scattering centers. Note that the resistivity of undoped graphene is not infinite but has been found to be approximately 6 kΩ, due to the effects of Zitterbewegung,[22,23] this feature however cannot be taken into account in the presented calculations.

If defect states cause a weak insulator-metal transition and allow for an increased conductivity, they must be sufficiently extended. This criterion leads to a critical defect concentration for when the system becomes metallic. In addition, defects induce impurity states and a corresponding change in the CPA-averaged DOS, which leads to a shift of the Fermi level in order to maintain charge neutrality (this can be viewed as accepting or donating charge to the defects). In order to investigate this effect in detail, we have compared the shifts in the DOS curves for different impurity concentrations.

This shift can be seen in Fig. 1 for two selected concentrations of impurities, 0.1% and 1%. It may be seen that the presence of impurities move the Fermi level into the valence band. Both the shift of the Fermi level and the presence of an impurity state, with an associated increased scattering, influence the conductivity and it is desirable to distinguish between contributions from these two effects. We have for this reason considered a model system as follows. The Green's function of the model system was kept identical to that of a graphene system with a very low concentration of defects (0.1%), but in the calculation of transport properties, a Fermi level corresponding to a much larger concentration of defects (1%) was used. This is in the spirit of the rigid band approximation. This system will in the rest of our paper be denoted as graphene II. Its conductivity is found to be greatly enhanced compared to the real graphene system with an impurity concentration of 0.1% even though the only difference is a 0.016 Ry change in the Fermi energy.

In a metallic regime the residual resistivity originates from impurity scattering and it is thus expected to be proportional to the impurity concentration. Graphene with $x=1\%$ and graphene II (with $x=0.1\%$) have as the main difference the amount of impurity scattering centers (contrary to the different conductivity regime of graphene with $x=0.1\%$). When the ratio of the resistivities between the two former systems is evaluated, it indeed conforms roughly the expected proportionality for metals. Overall the results indicate that the initial part of the resistivity curve in Fig. 4 is due to an increased metallic component of the electronic structure with negligible influence from impurity scattering. At higher defect concentrations (0.5% and above) the effect of the impurity scattering becomes important and the balance between these two effects causes the resistivity to saturate to a constant value for large defect concentrations.

The ground-state calculations show that the shift of the Fermi level depends on the amount of defects (x) approximately as the square root of x. This conforms the linear DOS of graphene near the Dirac point. For single-layer graphene we obtain $\Delta E_F = -0.24$ Ry $\sqrt{x}$.

3. Transport properties of bilayer graphene

For carbon systems with more than one layer of graphene, the dependence of defect concentration may be different. In addition, based on the discussion in the model section, it is of interest to study how defects in one layer influence the conducting properties of the other layer. For this reason, we calculated conductances in each layer of bilayer graphene (two graphene layers) separately. The calculated resistivity as a function of defect concentration in one of the layers is shown in Fig. 5 (the defect concentration of the other layer is held fixed at 0.1%). A strong decrease in the resistivity at $x < 0.3\%$ is again present, for both layers, but the resistivity in the metallic regime is somewhat higher than for single layer (cf. Fig. 3). Note that resistivities of both layers are strongly affected by the defect concentration and that the dependence of the defect-free layer is roughly similar to the layer with defects.

The initial behavior of Fig. 5, with a decrease in resistivity in both the layer with defects as well as the one without defects, is consistent with the model calculations presented here, where midgap states are introduced also in the defect-

free layer. In addition, since the Fermi levels must be equal in the two layers in equilibrium, an increased concentration of defects in one layer will introduce a shift of the Fermi level in both layers. The dependence of the shift on the defect concentration is approximately found to be $\Delta E_F = -0.19$ Ry $\sqrt{x_1+x_2}$, where x_1 and x_2 are defect concentrations in the first and second graphene layers, respectively. This implies a slightly larger charge transfer to vacancy states than in the case of single layer. Both the shift of the Fermi level as well as the appearance of midgap states cooperate to increase the conductivity for small defect concentrations. For higher concentrations it is again the impurity scattering which sets in and inhibits a continued increase in the conductivity. Note that this effect is present in both graphene layers, which implies that the increase in defects in one layer influences the self-consistent potential also of the other layer leading to an enhanced impurity scattering.

4. Transport properties of N-doped graphene

The calculated resistivity of a single-layer graphene with nitrogen impurities is shown in Fig. 6 as a function of N impurity concentration. Note that the trend in this figure is quite similar to the case of single-layer graphene with vacancies, a minimum in the resistivity is also found for around 0.5% N impurities. However the resistivity in the metallic regime is now lower, compared to that of vacancy defects, because nitrogen is not as strong scatterer as a vacancy defect, and the N atom provides electron carriers to the material and shifts Fermi level much more than vacancy defects.

IV. CONCLUSION

In this paper we demonstrate that impurities in monolayer and bilayer graphene heavily influence the transport properties. Our results show primarily that the impurities enhance significantly the conductivity of graphene in the limit of zero applied gate voltage, especially for low concentrations of impurities. For larger concentrations impurity scattering becomes more important, which hinders a continuous enhanced conductivity for impurity concentrations larger than 0.5%.

Our theoretical results are consistent with recent experimental observations[6] and provide a possible route for functionalizing the transport properties of graphene by chemical means. The microscopic mechanism behind this possibility is the appearance of midgap states, which enhances the metallic component to the density of states at the Fermi level, in combination with a shift of the Fermi level caused by vacancy defects as well as N defects.

The results from the tight-binding model suggest that the modified LDOS in the defected layer of a bilayer is enhanced around the Fermi level, as compared to the LDOS for clean single-layer graphene. For decreasing coupling $t_\perp$ between the layers, this enhancement turns into a peak, a midgap state, in agreement with earlier studies.

Finally, we demonstrate by means of both the tight-binding model and *ab initio* calculations that for a bilayer graphene, midgap states or a peaked LDOS appear in one layer even if defects are present only in the second layer. This is an interesting result as the electronic-structure and transport properties in the pure layer is affected by the presence of the layer with vacancy defects through a weak interaction. The magnitude of the peaked LDOS, or midgap state, is predicted to scale linearly with the coupling $t_\perp$ between the graphene layers by the tight-binding model. However, the distance and sublattice dependence of metallicity is more prominent in the defected layer than the pure layer. Thus one can envisage control of the properties of a pure graphene layer by manipulation with defects in another graphene layer in the vicinity.

ACKNOWLEDGMENTS

We acknowledge support from the Swedish Research Council, STINT, SNAC, and the Academy of Sciences of the Czech Republic (Grants No. KJB101120803, No. KAN400100653 and the computational cluster Luna). O.E. acknowledges the ERC for support.

[1] K. S. Novoselov, A. K. Geim, S. V. Morozov, D. Jiang, Y. Zhang, S. V. Dubonos, I. V. Grigorieva, and A. A. Firsov, Science **306**, 666 (2004).
[2] M. I. Katsnelson, K. S. Novoselov, and A. K. Geim, Nat. Phys. **2**, 620 (2006).
[3] A. H. Castro Neto, F. Guinea, N. M. R. Peres, K. S. Novoselov, and A. K. Geim, Rev. Mod. Phys. **81**, 109 (2009).
[4] V. A. Coleman, R. Knut, O. Karis, H. Grennberg, U. Jansson, R. Quinlan, B. C. Holloway, B. Sanyal, and O. Eriksson, J. Phys. D **41**, 062001 (2008).
[5] F. Schedin, A. K. Geim, S. V. Morozov, E. W. Hill, P. Blake, M. I. Katsnelson, and K. S. Novoselov, Nature Mater. **6**, 652 (2007).
[6] S. H. M. Jafri *et al.*, J. Phys. D **43**, 045404 (2010).
[7] T. O. Wehling, A. V. Balatsky, M. I. Katsnelson, A. I. Lichtenstein, K. Scharnberg, and R. Wiesendanger, Phys. Rev. B **75**, 125425 (2007).
[8] B. Sanyal, O. Eriksson, U. Jansson, and H. Grennberg, Phys. Rev. B **79**, 113409 (2009).
[9] I. Turek, V. Drchal, J. Kudrnovský, M. Šob, and P. Weinberger, *Electronic Structure of Disordered Alloys, Surfaces and Interfaces* (Kluwer, Boston, 1997).
[10] U. von Barth and L. Hedin, J. Phys. C **5**, 1629 (1972).
[11] A. K. Solanki, A. Kashyap, T. Nautiyal, S. Auluck, and M. A. Khan, Solid State Commun. **100**, 645 (1996).
[12] P. Soven, Phys. Rev. **156**, 809 (1967).
[13] B. Velický, S. Kirkpatrick, and H. Ehrenreich, Phys. Rev. **175**, 747 (1968).
[14] K. Carva, I. Turek, J. Kudrnovský, and O. Bengone, Phys. Rev. B **73**, 144421 (2006).
[15] J. Nilsson, A. H. C. Neto, F. Guinea, and N. M. R. Peres, Phys. Rev. Lett. **97**, 266801 (2006).

[16] N. M. R. Peres, F. Guinea, and A. H. Castro Neto, Phys. Rev. B **72**, 174406 (2005).
[17] Y. V. Skrypnyk and V. M. Loktev, Low Temp. Phys. **33**, 762 (2007).
[18] P. Hohenberg and W. Kohn, Phys. Rev. **136**, B864 (1964).
[19] G. Kresse and J. Hafner, Phys. Rev. B **47**, 558 (1993).
[20] G. Kresse and J. Furthmüller, Phys. Rev. B **54**, 11169 (1996).
[21] N. M. R. Peres, F. Guinea, and A. H. C. Neto, Phys. Rev. B **73**, 125411 (2006).
[22] K. S. Novoselov, A. K. Geim, S. V. Morozov, D. Jiang, M. I. Katsnelson, I. V. Grigorieva, S. V. Dubonos, and A. A. Firsov, Nature (London) **438**, 197 (2005).
[23] M. I. Katsnelson, Eur. Phys. J. B **51**, 157 (2006).